J. Electrochem. Sci. Eng. **8(3)** (2018) 205-217; DOI: http://dx.doi.org/10.5599/jese.495

Open Access : : ISSN 1847-9286

https://pub.iapchem.org/ojs/index.php/JESE

Original scientific paper

The template-assisted electrodeposition of platinum nanowires for catalytic applications

Soha Mohajeri✉, Abolghassem Dolati✉, Sahar Hashemi Daryan

Department of Materials Science and Engineering, Sharif University of Technology, Tehran, Iran

Corresponding authors - E-mail: ✉smohajeri@alum.sharif.edu, ✉dolati@sharif.edu

Received: January 6, 2018; Revised: February 13, 2018; Accepted: February 14, 2018

Abstract

Template-assisted electrodeposition technique was applied to synthesize platinum nanowires (Pt NWs) on polycarbonate templates (PCT) with pore diameters of 15, 50, and 100 nm for catalytic applications. Influences of sulfuric acid added to the electrolyte, different potential scanning rates and different pore diameters of templates on the electrodeposition process of Pt NWs were investigated by electrochemical techniques, including voltammetry and chronoamperometry methods. It was confirmed that at lower scan rates and in acidic solutions, electrodeposition of platinum on templates with larger pores is controlled by diffusion. The potential range for deposition of Pt NWs was determined and the potentiostatic technique was utilized by applying various potentials of different durations to fabricate the NWs. The morphological characteristics of Pt NWs were examined using the scanning electron microscopy (SEM). It was shown that the growth of Pt NWs on PCT 50 nm followed a pine-tree pattern, while the Pt NWs grew spherically on PCT 100 nm. The uniform and compact shape of Pt NWs was verified by the transmission electron microscopy (TEM). The catalytic activities of the prepared Pt NWs with the same exchanged charge density for hydrogen adsorption/desorption and methanol oxidation reactions were determined by the cyclic voltammetry (CV) testing, and the superior electrocatalytic performance was detected for Pt NWs prepared on PCT 50 nm. This enhanced catalytic activity was attributed to the higher surface-to-volume ratio, larger electrochemical active surface area and higher density of exposed active sites accessible on the pine-tree morphology of these Pt NWs compared to the spherical structure of Pt NWs fabricated on PCT 100 nm. This makes Pt NWs prepared on PCT 50 nm to be a promising catalyst for direct methanol fuel cells (DMFCs).

Keywords

Platinum nanowires; Polycarbonate templates; Electrodeposition; Hydrogen adsorption/desorption; Methanol oxidation reaction

Introduction

In recent years, noble-metal nanostructures have attracted extensive research attention due to their promising potentials for numerous electrocatalytic applications including a variety of fuel cell systems, electrochemical biosensors and batteries [1]. In particular, the synthesis of platinum-based nanostructures such as nanotubes, nanoparticles and nanowires with specific structural features has been an area of considerable interest [2]. This happened owing to the enhanced catalytic capabilities of platinum for applications in direct methanol fuel cells (DMFCs) which are considered as highly promising power sources for electric vehicles and portable electronic devices [3]. Limited supply and high cost of this precious metal, however, have impeded its commercial utilization. Moreover, the formation of intermediate species in the process of methanol oxidation tends to poison the Pt surface and diminish the oxidation rate, reducing thus the catalytic performance of this metal [4]. In order to improve the catalytic activity and the poisoning tolerance of Pt catalysts, various researchers have focused their investigations on the replacement of zero-dimensional (0D) Pt nanoparticles with one-dimensional (1D) Pt nanowires (Pt NWs) [5,6]. Several structural features offered by Pt NWs such as anisotropic morphology and high surface-to-volume ratio can enhance their mass-transport and electron-transfer kinetics, leading to the superior catalytic activity of Pt for hydrogen evolution and methanol oxidation reactions [7].

Although various techniques such as electron-beam deposition [8], solvothermal synthesis [9], physical vapor deposition [10], electron beam lithography [11] and plasma sputtering [12] have been applied to fabricate Pt NWs, electrodeposition [13] has been proven as the most commonly used deposition method due to its low cost and high productivity [14]. In particular, the template-based electrodeposition of Pt NWs has been established as an effective method due to its simplicity and high-yielding process. This method provides a well-organized approach for the fabrication of isolated nanowire arrays with uniform diameters determined by the pore diameter of the template [15]. It is generally accepted that the diameter of nanowires plays a fundamental role in their functionality. As the diameter of nanowires decreases, their surface-to-volume ratio increases and consequently, the variation of the surface energy significantly influences the surface state and the related physical and chemical properties [16]. Although many studies have investigated the template-based electrodeposition of Pt NWs, very few researchers have examined distinct morphological and structural properties of Pt NWs fabricated on templates with different pore diameters. Also, a limited research has so far been reported on the electrocatalytic activity of Pt NWs for hydrogen adsorption/desorption and methanol oxidation reactions.

The current study aims to examine the electrodeposition of Pt NWs on polycarbonate templates (PCT) with different pore diameters and determine the dependence of their electrochemical behavior and morphological properties upon the pore size of templates. The work has been focused on the hydrogen adsorption/desorption on Pt NWs and the influence of their diameter on the methanol oxidation reaction performances.

Experimental

The electrochemical deposition of Pt NWs was carried out in a typical three-electrode cell and the potential was recorded with reference to a saturated calomel electrode (SCE). A pure platinum plate with the surface area of 2×1 cm^2 was used as the counter electrode and polycarbonate templates (PCT) with the surface area of 0.2×1 cm^2, pore diameter of 15, 50, and 100 nm, pore length of 6 μ, and pore density of 10^8 pores/cm^2 were employed as the working electrode. In order to impart conductivity to the working electrode, the solution sides of the templates were coated

with 50 nm-thick Au layer via sputtering. Two electroplating baths were prepared and all the reagents were of analytical grade from Merck. In the first bath, 0.05 M H_2PtCl_6 was added drop-wise to deionized water-hydrochloric acid mixture (pH 1.6) under continuous stirring. In order to study the influence of sulfuric acid adding on the electrodeposition of Pt NWs, the second electroplating bath was prepared. 0.1 M H_2SO_4 was added to 0.05 M H_2PtCl_6 solution with vigorous mixing during addition, and the final solution was added drop-wise to a mixture of deionized water and hydrochloric acid with already adjusted pH of 1.6. Both electroplating baths were purged with N_2 at room temperature for 2 h. To optimize the deposition potentials suited for the deposition of Pt NWs, linear sweep voltammograms and chronoamperometry curves were recorded by an EG&G Princeton Applied Research (PAR) potentiostat and influences of 0.1M H_2SO_4 added to the electrolyte, different potential scanning rates, and different pore diameters of templates on the electrodeposition process of Pt NWs were investigated. Afterwards, the potential range for deposition of Pt NWs was determined and subsequently, the potentiostatic method was utilized by applying various potentials of different durations to synthesize the nanowires. The surface and cross-sectional morphologies of the obtained Pt NWs were examined by a scanning electron microscope (SEM, TESCAN Model), after dissolving the polycarbonate membranes by dichloromethane. A transmission electron microscopy (TEM, EM-10C Model) analysis was used to evaluate the Pt NWs nanostructure. The electrocatalytic activity of Pt NWs obtained with the same exchanged charge density was assessed in a cell containing the PC templates filled with the Pt NWs (working electrode, 0.2×1 cm^2) and a platinum sheet (counter-electrode, 2×1 cm^2). The supplied bias and current were controlled by an Autolab PGSTAT 302 electrochemical system. The cyclic voltammetry (CV) tests for hydrogen adsorption/desorption reactions were conducted in an argon-purged 0.5 M H_2SO_4 solution at room temperature under continuous stirring and the obtained CV curves were used to estimate the electrochemically active surface area (ECSA) of Pt NWs catalysts. The methanol oxidation reaction activity of Pt NWs was studied by CV tests in a 0.5 M H_2SO_4 electrolyte containing 2 M CH_3OH, and the optimum diameter of NWs for obtaining the maximal catalytic efficiency was determined.

Results and discussion

Electrochemical studies of the Pt NWs deposition

The influence of sulfuric acid added to the plating bath on the electrodeposition of Pt NWs was studied. Figure 1 demonstrates the cathodic voltammetry curves of PCT 50 nm working electrode, measured in a pure bath and H_2SO_4-containing solution in the potential range of 0 to −2000 mV *vs*. SCE at the scan rate of 5 mV/s. It can be observed that in the presence of the sulfuric acid, higher current densities were measured and the curve shifts to more positive potentials. The higher value of slope indicates that the electrodeposition of Pt ions occurs at a higher rate in a H_2SO_4-containing bath compared to the pure deposition bath, depicting that the sulfuric acid plays a catalytic role in the deposition of Pt NWs.

In order to investigate the effect of various potential scan rates on the electrodeposition of Pt NWs, the linear voltammetry curves recorded in a H_2SO_4-containing solution in the range of 0 to -1000 mV *vs.* SCE at the scan rates of 20, 50 and 100 mV/s are illustrated in Figure 2. Two irreversible peaks can be detected in the cathodic branches of the curves obtained at the scan rates of 20 and 50 mV/s. The peaks are ascribed to the successive reduction of Pt^{4+} to Pt^{2+} ions and of Pt^{2+} ions to Pt, respectively, according to the following reactions:

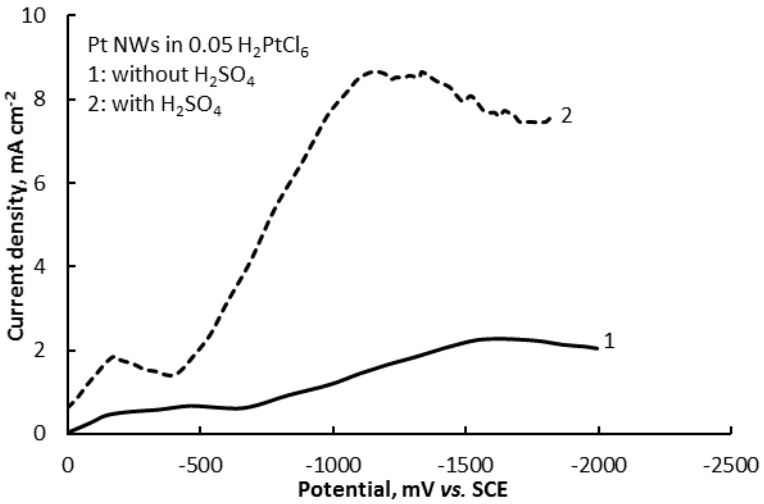

Figure 1. *Effect of 0.1 M H_2SO_4 added to the plating bath on electrodeposition of Pt NWs on PCT 50 nm at the scan rate of 5 mV s^{-1}*

$$[PtCl_6]^{2-} + 2e^- \rightarrow [PtCl_4]^{2-} + 2Cl^- \quad (1)$$

$$[PtCl_4]^{2-} + 2e^- \rightarrow Pt + 4Cl^- \quad (2)$$

A typical feature of the diffusion-controlled electrodeposition is that an increase of the scan rate shifts the reduction peaks to more negative potentials and causes higher current densities along with a simultaneous increase in the deposition rates. This behavior can be attributed to the fact that at higher scan rates, the cations have a lower opportunity for deposition on the surface and therefore need a higher energy and overpotential for deposition. Figure 2, depicts such a feature, suggesting that the electrodeposition of Pt is under the mass transfer control. With the increase of the scan rate from 20 to 50 mV/s, the mass transfer is enhanced, leading to the intensified adsorption of platinum ions on the working electrode. Consequently, the potential difference between the cathodic peaks increases. Finally, at the scanning rate of 100 mV/s, a single wide peak is observed due to the lack of the deposition duration that leads to the decrease of the deposited platinum species on the cathode.

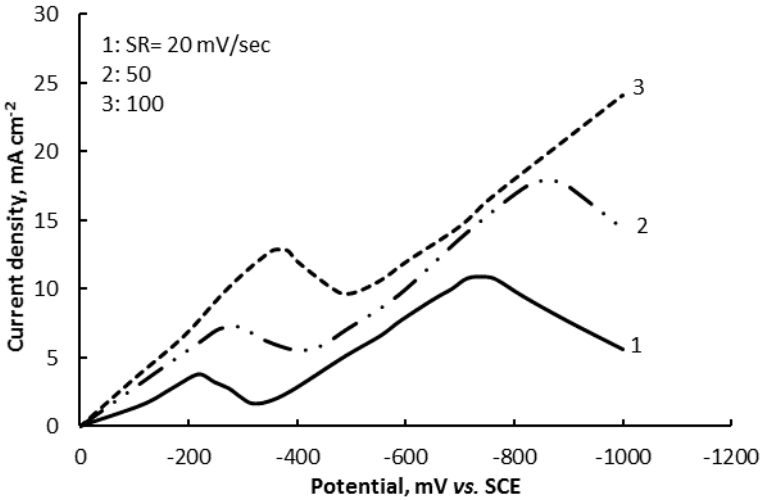

Figure 2. *Linear sweep voltammograms of Pt NWs deposited on PCT 50 nm at different scan rates.*

The influence of the template pore diameter (15, 50, and 100 nm) on the linear voltammetric curves in the range of 0 to -1000 mV *vs*. SCE at a scan rate of 50 mV/s is depicted in Figure 3. No diffusion peaks were observed for deposition on PCT 15 nm and therefore, it can be concluded that the charge transfer governs the system kinetics. This can be attributed to the higher surface-

to-volume ratio of the small pores with the diameter of 15 nm, which provides facile pathways for mass transfer and more effective exposure of active surface sites for the progressive ions flux to the cathode surface. Thus, the diffusion of the solution species is fast and the deposition current is restricted by the electron transfer at the working electrode. This is a characteristic of deposition reactions in which the charge transfer is rate determining [17,18]. However, for PCT 50 and 100 nm, diffusion controls the curves. The increase of pore diameters leads to the increase of the deposition current density and shifts the curves to more negative potentials. This can be due to the larger size of the pores and transference of more platinum ions into the pores, which requires higher overpotentials for reduction.

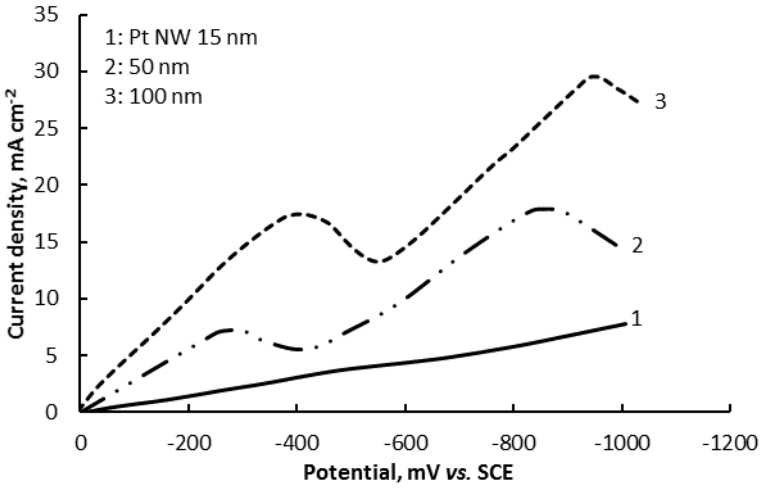

Figure 3. *Linear sweep voltammograms for electrodeposition of Pt NWs on templates with different pore diameters at scan rate of 50 mV* s^{-1}

Figure 4 illustrates the potentiostatic *i-t* transients of Pt NWs deposited on PCT 50 and 100 nm at −400 mV *vs*. SCE. Based on the characteristic shape of the chronoamperometry curves, a nucleation and growth mechanism can describe the electrodeposition process having the rate of growth limited by diffusion [19]. At the initial times, the current density increases due to the nucleation process and 3D growth of the nuclei. Subsequently, diffusion controls the current drops and the deposition. Finally, the current density remains relatively constant and filling up the pores occurs. These curves also reveal that the deposition trend does not change as the pores diameters increase from 50 to 100 nm.

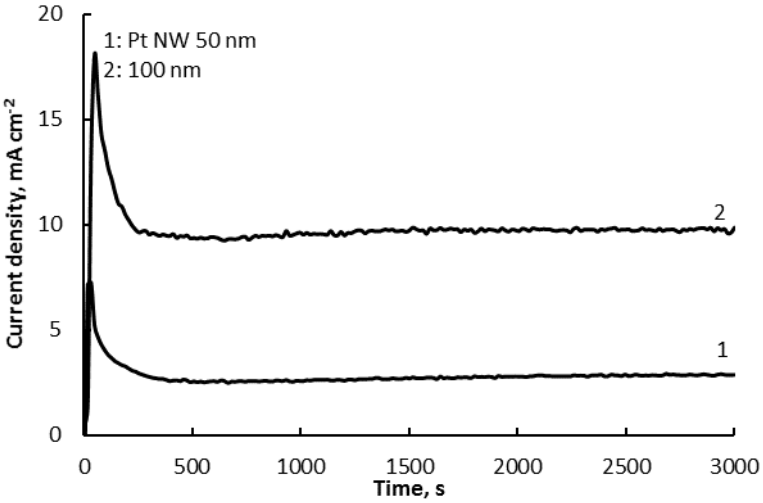

Figure 4. *Chronoamperometry curves for deposition of Pt NWs on PCT 50 and 100 nm at −400 mV* vs. *SCE.*

Morphological study of Pt nanowires

From the linear sweep voltammetry curves shown in Figure 3, the reduction potential region for the deposition of Pt NWs on templates with pore diameters of 50 and 100 nm can be determined. Due to the locations of peaks in the diffusion-controlled electrodeposition of nanowires, the values of −250 and−400 mV were determined as the starting potentials for the deposition of Pt NWs on PCT 50 and 100 nm, respectively. The potentiostatic method was utilized to synthesize the nanowires by applying various potentials in the range of −250 to −400 mV for different durations.

Morphologies of Pt NWs deposited on the PCT 50 nm from a H_2SO_4-containing solution at different potentials in the range of −250 to −400 mV for 500 s were analyzed by SEM. In order to study the surface morphology of prepared Pt NWs, the deposited samples were cut, and the surface areas of the templates were locally dissolved in CH_2Cl_2. Figures 5 (a)–(c) illustrate the cross-sectional SEM images of Pt nanowires grown on PCT 50 nm at −250, −350 and −400 mV, respectively. Figures 5 (d)–(f) show the SEM images at a higher magnification, and it can be observed that the average lengths of the nanowires vary between 1 to 4.5 µ. According to Figures 5 (a) and (d), it can be observed that at −250 mV, the growth of nanowires is uniform but due to the lack of deposition time, they do not meet the surface of the template. In Figures 5 (b) and (e), it seems that at increased applied potential to −350 mV, the holes are not completely filled due to the short deposition time, but the growth of nanowires occurs simultaneously and uniformly. Figures 5 (c) and (f) demonstrate that at more negative potential of −400 mV, due to the hydrogen evolution reaction, the efficiency of the nanowires deposition declines, leading to a less uniform growth of nanowires.

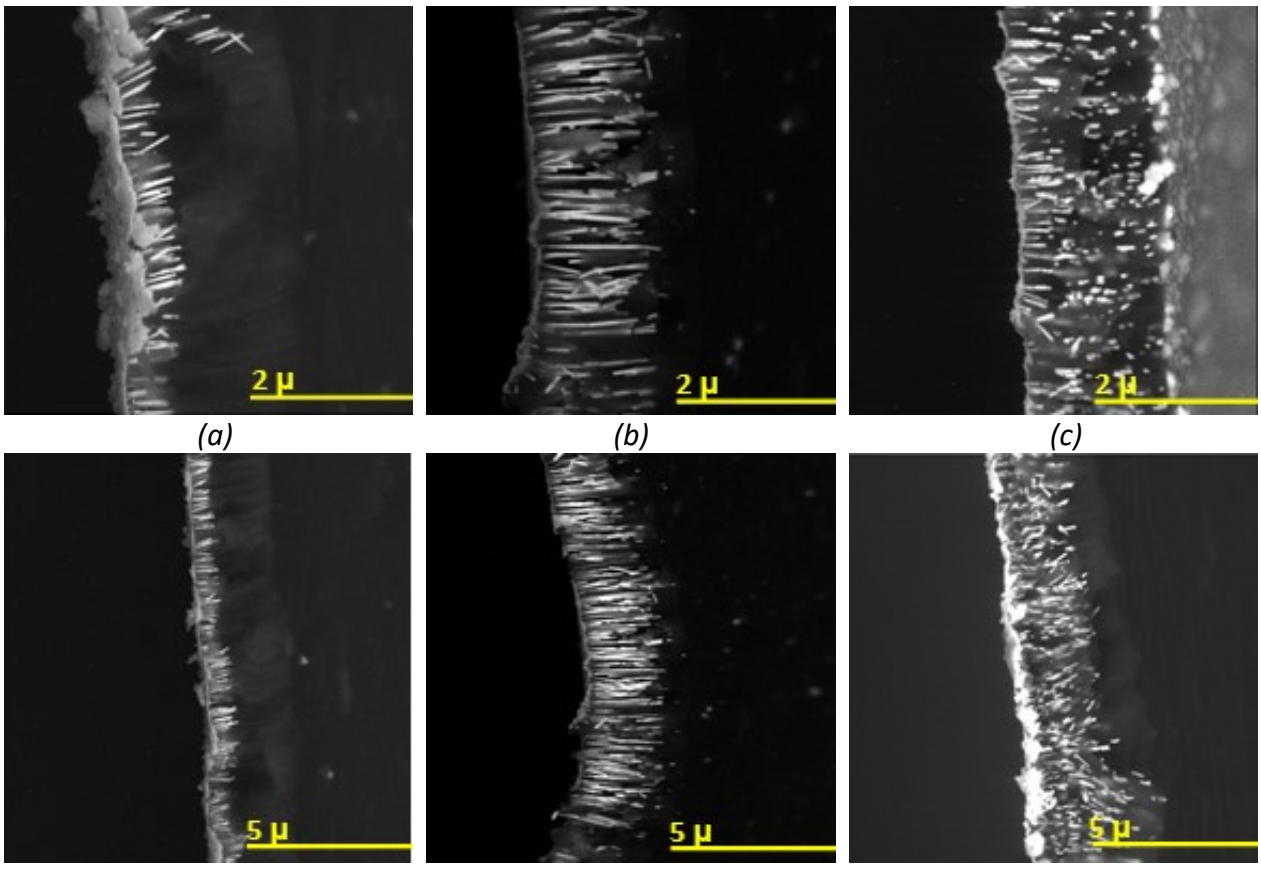

(a) *(b)* *(c)*

(d) *(e)* *(f)*

Figure 5. *SEM images of PT NWs electrodeposited for 500 s on PCT 50 nm at the potential of: (a), (d) –250, (b), (e) –350, and (c), (f) –400 mV.*

In order to examine the consequences of increasing the deposition duration on the surface and cross-sectional morphology of Pt NWs deposited on PCT 50 and 100 nm, the potentials of –350 and –400 mV were applied for 3000 s. According to Figures 6 (a) and (b), Pt NWs deposited on PCT 50 nm at –350 mV, represent the tree branches and resemble pine needles.

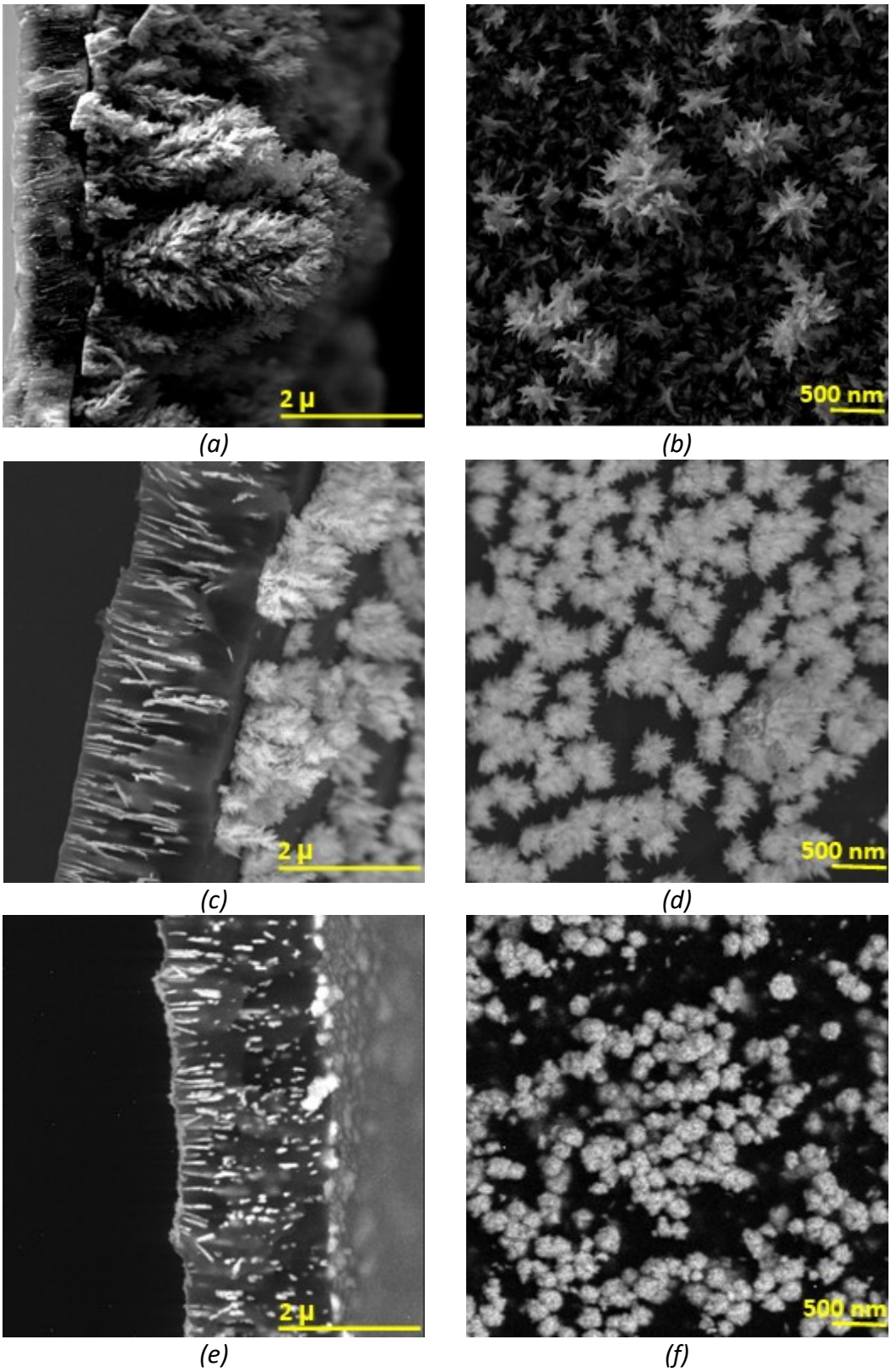

Figure 6. *Surface and cross-sectional morphology of Pt NWs electrodeposited for 3000 s on PCT 50 nm at the potential of (a), (b) –350, (c), (d) –400 mV, and on PCT 100 nm at the potential of (e), (f) –400 mV.*

This pine-tree morphology can be attributed to the tendency of the multifaceted platinum nuclei to branch, spread, and dramatically overgrow on the surface. It is noteworthy to mention that unlike the nanowires of other fcc metals such as gold, copper, nickel, and cobalt, the Pt NWs do not follow a cauliflower growth pattern and do not tend to form caps on the surface of the templates. Alternatively, they continue their overgrowth rather than overlapping, and manifest pine-tree structures that are single crystalline, and their facets grow close to the {001} plane [20]. As depicted in Figures 6 (c) and (d), at the potential of −400 mV, the Pt NWs on the PCT 50 nm do not grow uniformly along the pores, reaching the surface of the template and continuing their growth on the surface. As mentioned before, the evolution of hydrogen at more negative potentials accounts for the non-uniform growth of platinum nanowires. Figures 6 (e) and (f) demonstrate the spherical growth of Pt NWs on the PCT 100 nm.

It was confirmed that the nucleation process of Pt NWs on both PCT 50 and 100 nm follow the instantaneous mechanism in which the rate of new nuclei formation at the initial stage of deposition is high enough to immediately activate all the nucleation sites. However, the number of nuclei remains constant during the growth process and the 3D growth of the nuclei is limited by diffusion [21]. With regards to Figures 6 (d) and (f), at the same deposition potential of −400 mV, the ratio of surface-to-volume of Pt NWs prepared on PCT 50 nm is larger than those deposited on PCT 100 nm, and the driving force inside the smaller pores is higher, leading to the increase of nucleation density inside the pores with the size of 50 nm. On the other hand, the mass transport inside smaller pores with the size of 50 nm is more limited by diffusion in comparison to the pores with the size of 100 nm. Thus, the diffusion coefficient is smaller in PCT 50 nm and the 3D growth of the nuclei follows a pine-tree pattern. As the 3D growth inside the pores of PCT 100 nm is less restricted by diffusion and due to the lower concentration gradient inside larger pores, the nuclei are promoted to grow spherically on the PCT 100 nm.

The influence of the pore size of templates on the length of nanowires deposited under the potential of −400 mV during 2000 s is represented in Figure 7. Due to the dissolution of polycarbonate membranes by dichloromethane, the nanowires are randomly distributed on the surface.

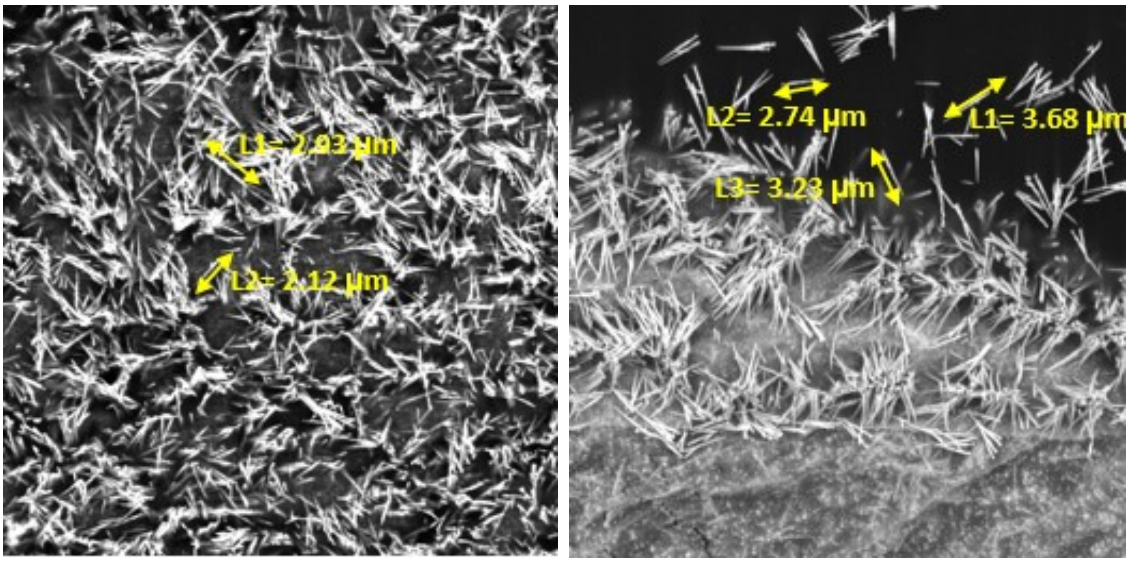

(a) *(b)*

Figure 7. *Surface morphology of Pt NWs electrodeposited at the potential of −400 mV for 2000 s on PCT: (a) 50 and (b) 100 nm.*

The relatively short duration of applying the deposition potential resulted in the incomplete filling of the pores, and the average length of nanowires on PCT 50 (Fig. 7(a)) and 100 nm (Fig. 7(b)) are 2.5 and 3.3 μ, respectively. Since the system is controlled by diffusion at −400 mV, the efficient surface area and the diffusion coefficient are higher in bigger pores [13], leading to the formation of longer nanowires.

TEM characterization of Pt nanowires

TEM images of Pt NWs deposited on the PCT 50 nm at −400 mV for 1000 s are depicted in Figure 8. According to Figure 8 (a), under the magnification of 1500, the nanowires are uniform, and their diameter is 100 nm. Due to the short deposition duration, the lengths of these nanowires are in the range of 1.5−2.5 μ, and they do not reach the thickness of template (6 μ). Figure 8 (b) depicts a uniform and compact nanowire having a diameter between 100 to 120 nm at different points. Since the end part of this nanowire is smaller and the deposition time is shorter than the required time for filling the pores, it can be concluded that this section belongs to the growing part of the nanowire. The dispersed grains inside the nanowire pertain to the growing nuclei and confirm that the nucleation and growth mechanism of nanowires are instantaneous and three dimensional, respectively.

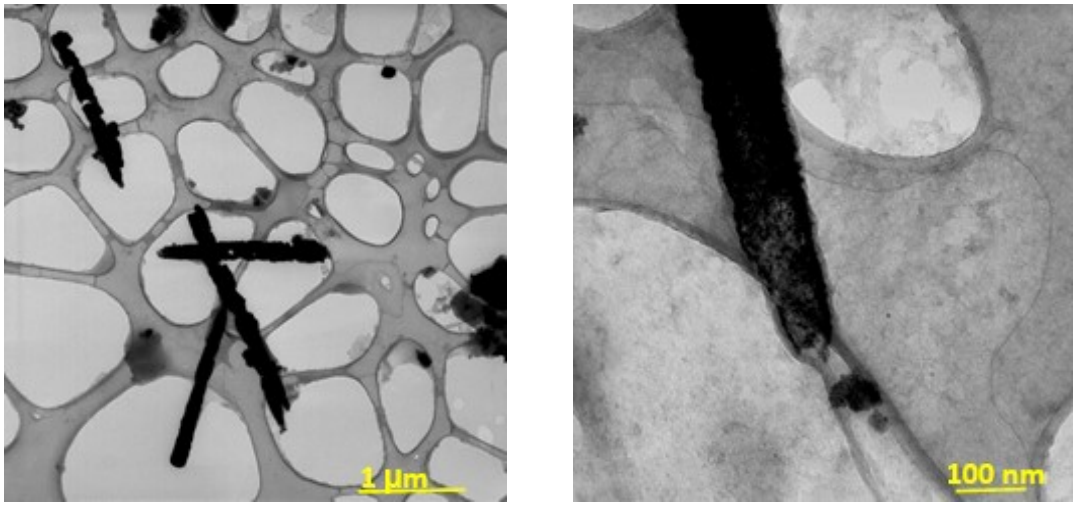

(a) *(b)*

Figure 8*. TEM images of Pt NWs electrodeposited for 1000 s at the potential of −400 mV on PCT 50 nm under the magnification of: (a) 1500 and (b) 8800*

Electrocatalysis in acidic solutions

In order to investigate the catalytic activity of Pt NWs 50 and 100 nm, the deposits obtained with the same exchanged charge density were compared. Based on Figure 4, the integration of chronoamperometric reduction current recorded over 3000 s for the Pt NWs 50 nm yielded the same amount of the exchanged charge as for the Pt NWs 100 nm recorded over 860 s. Therefore, Pt NWs prepared at the potential of −400 mV for 3000 s on PCT 50 nm and for 850 s on PCT 100 nm were selected for studying the influence of nanowires diameter on their electrocatalytic activity.

Adsorption/desorption of hydrogen

The cyclic voltammograms shown in Figure 9 compare the hydrogen adsorption/desorption performance of Pt NWs deposited at the potential of −400 mV for 3000 s on PCT 50 nm and for 850 s on PCT 100 nm, in a 0.5 M H_2SO_4 solution at a scan rate of 50 mV/s. Both catalysts display

peaks associated with the strong and weak adsorption/desorption of hydrogen molecules in anodic and cathodic sweeps in the sulfuric acid solution [22]. The existence of multiple peaks in both the cathodic and anodic scans, instead of one broad peak, reveals that various crystallographic planes of platinum participated in the reactions [23]. The upward and downward peaks are ascribed to hydrogen desorption (P^d_1 and P^d_2) and (P^a_1 and P^a_2) adsorption, respectively. Since the hydrogen desorption peaks for Pt NWs 50 nm are approximately 10 to 30 mV more negative than that of Pt NWs 100 nm, it can be concluded that the hydrogen binding energy is lower on the nanowires prepared on PCT 50 nm. The inferior hydrogen binding energy expedites the hydrogen desorption from the surface of nanowires and consequently, enhances the catalytic performance of nanowires. Moreover, the potentials of hydrogen adsorption peaks on Pt NWs 50 nm are more negative, and their current values are higher compared with those of Pt NWs 100 nm. This implies that a great quantity of hydroxide species is produced on the electrode. Furthermore, the integration area of hydrogen desorption peaks for Pt NWs 50 nm surpasses the Pt NWs 100 nm, indicating the higher amount of active surface area and thus, the more enhanced catalytic performance of the nanowires prepared on PCT 50 nm.

The electrochemical active surface area (ECSA) of Pt NWs was estimated from the area of desorption of atomic hydrogen on the CV curves in Figure 9, between 0 and -300 mV, via the following equation [24]:

$$\text{ESCA} = \frac{Q_H}{mc} \tag{3}$$

In eq. (3), Q_H is the total charge (mC cm^{-2}), m is actual Pt loading (mg cm^{-2}) on the substrate, and c signifies the charge required to oxidize a monolayer of hydrogen on a Pt surface (0.21 mC cm^{-2}). The ECSA values of Pt NWs 50 and 100 nm are calculated to be 51.32 and 44.56 m^{2}g^{-1}, respectively, indicating that Pt NWs 50 nm are capable of exposing sufficient active sites to guest molecules, leading to their superior electrocatalytic activity. This behavior can be due to the larger surface-to-volume ratio of Pt NWs 50 nm, as well as their unique pine-tree morphology (Fig. 6) which improves the surface roughness and increases the surface tendency for reaction with hydrogen.

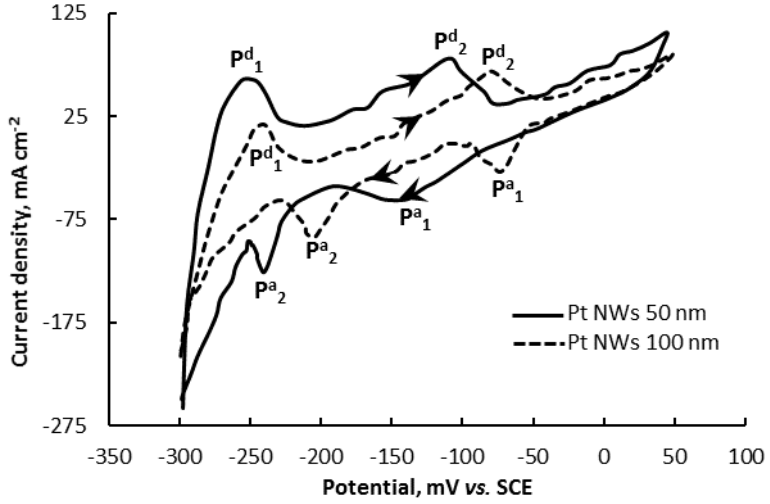

Figure 9. *Cyclic voltammograms of Pt NWs 50 and 100 nm in 0.5 M H_2SO_4 solution at scan rate of 50 mV s^{-1}*

Methanol oxidation

The CV curves presented in Figure 10 display the methanol oxidation performance of Pt NWs deposited at the potential of −400 mV for 3000 s on PCT 50 nm and for 850 s on PCT 100 nm, in a

0.5 M H_2SO_4 + 2 M CH_3OH solution. It can be observed that in the anodic scans, the methanol oxidation reactions begin at 230 and 473 mV for Pt NWs 50 and 100 nm, respectively. The onset oxidation potential for Pt NWs 50 nm is less positive compared to that of Pt NWs 100 nm, indicating that the morphology of Pt NWs 50 nm reduces the required initial potential and promotes the methanol oxidation. With the increase of the potential in the anodic sweep, the methanol molecules are dissociatively chemisorbed on Pt nanowires. As the potential is swept toward more anodic values, the anodic P_1 peaks emerge at 920 and 1032 mV for Pt NWs 50 and 100 nm, respectively. These peaks are attributed to the production of intermediates, poisonous Pt=C=O species, and carbon dioxide on the surface of the electrode. The lower value of the potential at P_1 peak for Pt NWs 50 nm in comparison to Pt NWs 100 nm is indicative of the reduced required potential for methanol oxidation on smaller nanowires. Moreover, the current value at P_1 peak for Pt NWs 50 nm is higher than that of Pt NWs 100 nm, which can be justified by the unique pine-tree morphology of nanowires and their larger ratio of surface-to-volume, leading to the higher accessibility of these nanowires for trapping the guest molecules. Thus, the adsorption of intermediate species on the surface of the Pt NWs 50 nm is enhanced and the methanol oxidation is intensified.

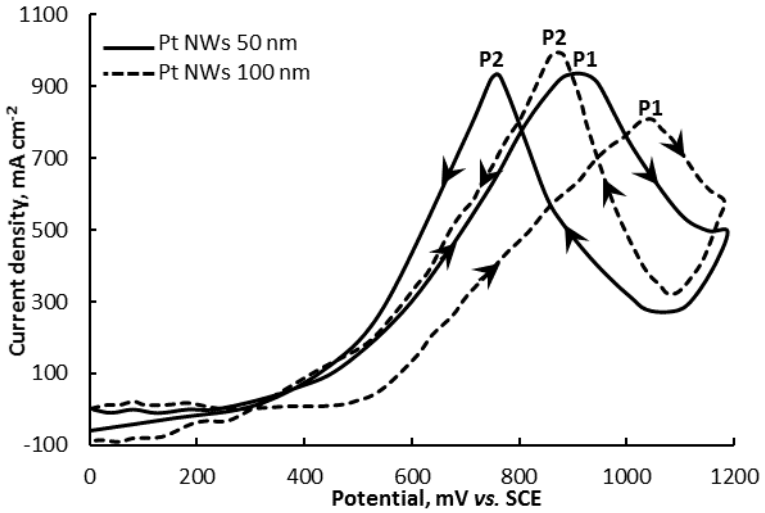

Figure 10. *Cyclic voltammetry curves for methanol oxidation on Pt NWs 50 and 100 nm in a solution containing 0.5 M H_2SO_4 and 2 M CH_3OH at scan rate of 50 mV s^{-1}*

In the backward scan, the cathodic P_2 peaks can be observed at 756 and 867 mV for Pt NWs 50 and 100 nm, respectively, due to the removal of poisonous Pt=C=O species. It is obvious that the P_2 peak appears at a more positive potential and with a higher current value for Pt NWs 100 nm compared to Pt NWs 50 nm. This is due to the higher amount of Pt=C=O species produced on Pt NWs 100 nm during the forward scan. Therefore, their oxidation is more difficult and requires higher potential and current values. Although Pt NWs act as effective catalysts for methanol oxidation, they tend to be poisoned by carbon monoxide [25]. The higher ratio of currents at P_1 peak to P_2 peak represents the improved tolerance of nanowires toward the poisoning by carbon monoxide [26]. Regarding Figure 10, this ratio is estimated to be 1.02 and 0.78 for Pt NWs 50 and 100 nm, respectively, demonstrating that the Pt NWs 50 nm possess an enhanced poisoning tolerance. This feature, in addition to the reduced onset and P_1 peak potentials leads to the enhanced electrocatalytic activity of these nanowires. The superior electrocatalytic performance of the nanowires prepared on PCT 50 nm is attributed to the higher value of surface-to-volume ratio of these nanowires, providing more uncovered active sites for trapping methanol molecules

for their subsequent oxidation. Furthermore, the pine-tree morphology of Pt NWs 50 nm provides enhanced electrocatalytic efficiency in comparison to the spherical morphology of Pt NWs 100 nm.

Conclusion

The platinum nanowires with different diameters were fabricated by the template-assisted electrodeposition technique. The deposition process was characterized by the voltammetry method and it was confirmed that addition of sulfuric acid to the plating bath accelerates deposition of Pt NWs. The influence of different potential scan rates on the electrodeposition of Pt NWs was investigated. It was observed that at low scan rates, two cathodic peaks appeared in the cyclic voltammetric curves, implying that the diffusion-controlled reduction of platinum ions occurred through two successive steps. However, at high scan rates, the presence of one cathodic peak on the voltammograms proved the incomplete and direct reduction of ions. The linear voltammetric curves obtained for different templates revealed that while the deposition was under charge transfer control on PCT 15 nm, the diffusion-controlled deposition occurred on PCT 50 and 100 nm. Morphological studies of NWs synthesized by the potentiostatic deposition technique revealed that at short deposition durations and under less negative deposition potentials, the growth of nanowires occurred simultaneously and uniformly. Less uniform growth of nanowires took place under more negative potentials due to the hydrogen evolution reaction. Moreover, at longer deposition durations, the platinum nanowires on PCT 50 and 100 nm possessed pine-tree and spherical structures, respectively. Based on the CV curves obtained in acidic solutions for deposits with an identical exchanged charge, the nanowires grown on PCT 50 nm exhibited enhanced catalytic performance toward hydrogen adsorption/desorption and methanol oxidation reactions compared to nanowires deposited on PCT 100 nm. This was ascribed to the higher surface-to-volume ratio, larger electrochemical active surface area, and the higher density of exposed active sites available on the pine-tree structure of Pt NWs 50 nm.

References

[1] K. I. Ozoemena, *Royal Society of Chemistry* **6** (2016) 89523-89550.
[2] E. P. Lee, Y. Xia, *Nano Research* **1** (2008) 129-137.
[3] G. R. O. Almeida, E. M. Sussuchi, C. T. D. Meneses, G. R. Salazar-Banda, K. I. B. Eguiluz, *International Journal of Electrochemical Science* **12** (2017) 7502-7517.
[4] W. Liu, J. Huang, *Journal of Power Sources* **189** (2009) 1012-1015.
[5] K. Tao, J. Wang, Y. Li, D. Xia, H. Shan, H. Xu, J. R. Lu, *Scientific Reports* **3** (2013) 1-6.
[6] Y. Lu, S. Du, R. Steinberger-Wilckens, *Applied Catalysis B: Environmental* **164** (2015) 389-395.
[7] S. Sun, G. Zhang, D. Geng, Y. Chen, R. Li, M. Cai, X. Sun, *Angewandte Chemie International Edition* **50** (2011) 422-426.
[8] L. Rotkina, *Applied Physics Letters* **83** (2003) 4426-4428.
[9] B. Y. Xia, H. B. Wu, Y. Yan, X. W. Lou, X. Wang, *Journal of the American Chemical Society* **135** (2013) 9480-9485.
[10] L. A. Dobrzanski, M. Szindler, M. Pawlyta, M. M. Szindler, P. Boryło, B. Tomiczek, *Open Physics* **14** (2016) 159-165.
[11] A. M. Contreras, J. Grunes, X. M. Yan, A. Liddle, G. A. Somorjai, *Catalysis Letters* **100** (2005) 115-124.
[12] P. Brault, A. Caillard, S. Baranton, M. Mougenot, S. Cuynet, C. Coutanceau, *ChemSusChem* **6** (2013) 1168-1171.
[13] S. S. Mahshid, A. Dolati, S. Hashemi Daryan, M. Ghorbani, *ECS Transactions* **28** (2010) 25-35.
[14] G. Nabiyouni, K. Hedayati, *Journal of Experimental Nanoscience* **9** (2014) 186-196.
[15] X. Z. Gong, J. N. Tang, J. Q. Li, Y. K. Liang, *Transactions of Nonferrous Metals Society of China* **18** (2008) 642-647.
[16] W. B. Yu, G. Ouyang, *Scientific Reports* **7** (2017) 1-7.

[17] J. M. Nugent, K. S. V. Santhanam, A. Rubio, P. M. Ajayan, *Nano Letters* **1** (2001) 87-91.
[18] E. Broaddus, J. Brubaker, S. A. Gold, *International Journal of Electrochemistry* **2013** (2013) 1-7.
[19] S. Mohajeri, A. Dolati, M. Ghorbani, *Journal of Ultrafine Grained and Nanostructured Materials* **49** (2016) 51-63.
[20] J. Chen, B. Lim, E. P. Lee, Y. Xia*, Nano Today* **4** (2009) 81-95.
[21] Y. J. Song, S. B. Han, K. W. Park, *Materials Letters* **64** (2010) 1981-1984.
[22] E. S. V. Neto, M. A. Gomes, G. R. Salazar-Banda, K. I. B. Eguiluz, *International Journal of Hydrogen Energy* **43** (2018) 178-188.
[23] S. Sun, G. Zhang, D. Geng, Y. Chen, M. N. Banis, R. Li, M. Cai, X. Sun, *Chemistry-A European Journal* **16** (2009) 829-835.
[24] H. A. Gasteiger, S. S. Kocha, B. Sompalli, F. T. Wagner, *Applied Catalysis B: Environmental* **56** (2005) 9-35.
[25] S. M. Alia, S. Pylypenko, K. C. Neyerlin, S. S. Kocha, B. S. Pivovar, *Journal of The Electrochemical Society* **162** (2015) 1299-1304.
[26] C. Xu, L. Wang, R. Wang, K. Wang, Y. Zhang, F. Tian, Y. Ding, *Advanced Materials* **21** (2009) 2165-2169.